Discovery of antibiotics and their targets in multidrug-resistant bacteria

Bakker, A.T.

Chapter 6

Isoquinoline sulfonamides are DNA gyrase inhibitors with an unprecedented binding mode

Introduction

In Chapter 5, LEI-800 (Figure 6.1), an isoquinoline sulfonamide, was discovered as a Gram-negative antibiotic as part of a hit optimization program, along with LEI-801 as an antibacterially inactive distomer. LEI-800 showed strong antibacterial activity against *Escherichia coli* and *Klebsiella pneumoniae*. Furthermore, LEI-800 also was effective against multidrug resistant clinical isolates of *E. coli*. This is important, as resistant Gram-negative infections are amongst the 21st centuries biggest global health threats, and treatment options with a novel mode-of-action (MoA) are urgently required.[1–3] As LEI-800 resulted from a phenotypic hit optimization effort, its MoA is unknown.

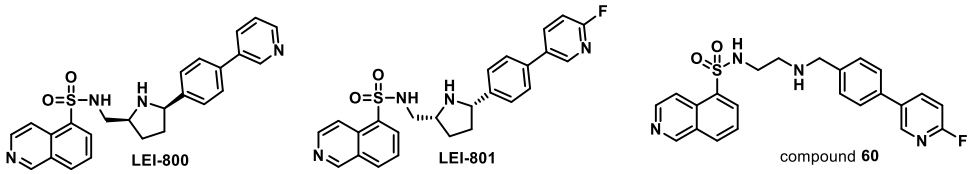

Figure 6.1 | LEI-800, LEI-801, and compound **60** comprise the isoquinoline sulfonamides in this chapter.

In this chapter, the MoA of LEI-800 is described. Bacterial cytological profiling (BCP) in combination with whole-genome sequencing of resistant strains, biochemical and structural biology studies using LEI-800 and LEI-801, led to the identification of the target and MoA of isoquinoline sulfonamides.

Results

Bacterial cytological profiling reveals distinct morphological profile of LEI-800. To gain more information about the MoA of LEI-800, an imaging-based approach termed bacterial cytological profiling (BCP), developed by Pogliano and co-workers, was employed[4] This method exploits the fact that bacteria often undergo drastic morphological changes as a result of antibiotic treatment and that antibiotics with differing MoAs result in visually distinct phenotypes. BCP allows for the quantification of these different phenotypes and, by constructing a reference map of antibiotics, the phenotypic similarity of cells treated with LEI-800 was compared to cells treated with a number of clinically-used reference antibiotics. To this end, the morphological effects of LEI-800 on *E. coli* were compared to a known cell wall synthesis inhibitor (ampicillin (AMP)), an RNA synthesis inhibitor (rifampicin (RIF)), a protein synthesis inhibitor (tetracycline (TET)), a DNA synthesis inhibitor (CIP) along with negative control (DMSO treatment) as well as a structurally similar inactive control (LEI-801).

To visualize these changes with fluorescence microscopy, the treated bacteria were stained with a membrane permeable DNA dye (DAPI), a lipophilic membrane dye (FM4-64) and a membrane impermeable DNA dye to signify loss of membrane integrity (SYTOX Green) (Figure 6.2A). Clear morphological changes were seen in response to all active compounds. Notably, LEI-800 induced elongation of the bacteria and condensation of the DNA, which resembled to some extent the effects observed in bacteria treated with CIP (Figure 6.2A). To obtain a more quantitative image analysis, 24 features that describe cell dimensions and fluorophore intensities of individual bacteria, were extracted (Table S6.1).

Principle component analysis of these 24 features revealed that the inactive control LEI-801 clustered with DMSO, while the reference antibiotics clustered separately from one another (Figure 6.2B,C). LEI-800 formed a cluster by itself, which was interesting considering its apparent similarity to CIP. This led to the suggestion that LEI-800 may have a unique MoA related to the inhibition of DNA synthesis.

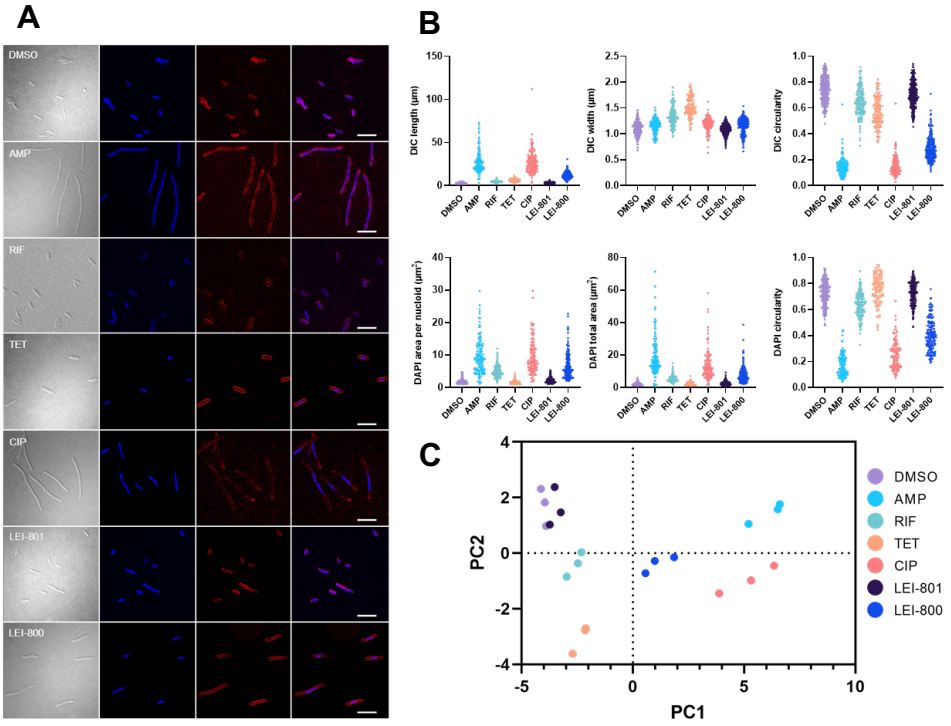

Figure 6.2 | Bacterial cytological profiling. A) Microscopy images of *E. coli* BW25113 from the BCP experiment. Conditions are, from top to bottom: DMSO, ampicillin (AMP), rifampicin (RIF), tetracycline (TET), ciprofloxacin (CIP), LEI-801, LEI-800. From left to right the channels indicate: DIC, DAPI, FM4-64, and DAPI/FM4-64 ovae. The bacteria treated with LEI-801 displayed a phenotype that is consistent with the DMSO control, while incubation with LEI-800 led to a phenotype resembling the ciprofloxacin and tetracycline morphological profile. Scale bars represent 10 µm. **B)** Individual graphs of six exemplary features extracted from BCP microscopy pictures after image analysis. Each dot represents the measured value for an individual bacterium. **C)** PCA plot of all the morphological features extracted from three independent BCP experiments.

Genomic studies reveal DNA gyrase as target of LEI-800. To identify the cellular target of LEI-800, the aim was to obtain drug-resistant mutants and subsequently to perform comparative genomics studies to identify single nucleotide polymorphisms (SNPs) that correlate to the resistance phenotype. To this end, *E. coli* (10^7 CFU) were plated on solid agar containing compound **60** (5x MIC) (Figure 6.3A) and nine viable colonies were isolated and screened for resistance (Figure 6.3B). All colonies had at least an 8-fold increase in MIC for compound **60** and cross-resistance was also subsequently found with LEI-800, while no cross-resistance was found with common antibiotics (Table S6.3). Of interest, one of the colonies showing resistance to **60** exhibited an enhanced sensitivity towards LEI-800.

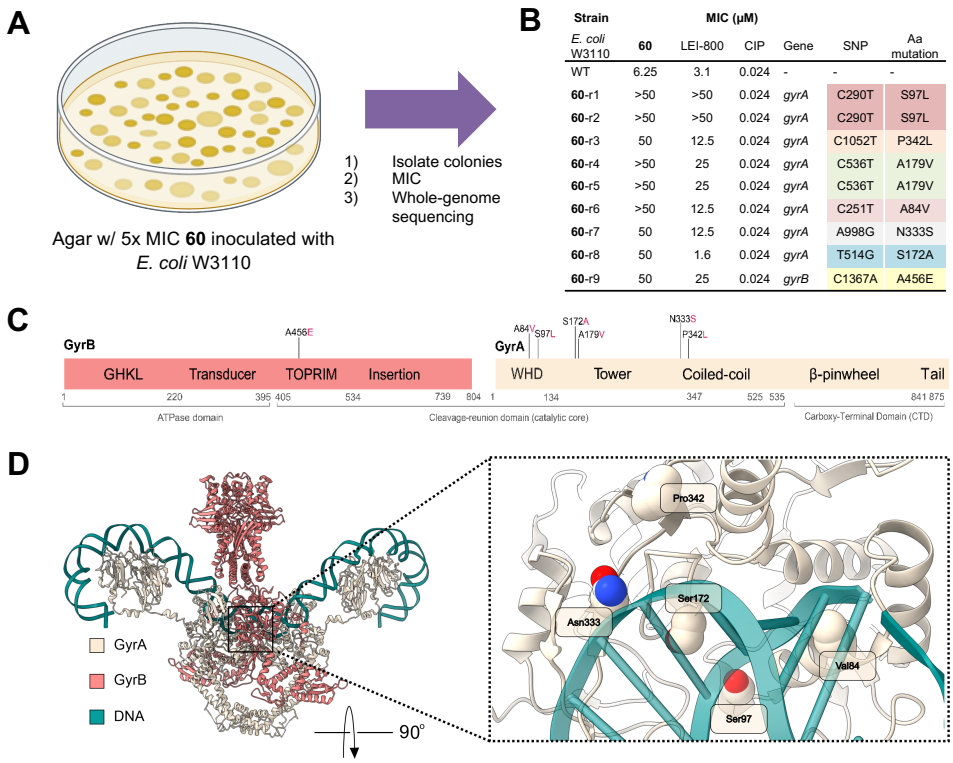

Strain	MIC (μM)					
E. coli W3110	**60**	LEI-800	CIP	Gene	SNP	Aa mutation
WT	6.25	3.1	0.024	-	-	-
60-r1	>50	>50	0.024	*gyrA*	C290T	S97L
60-r2	>50	>50	0.024	*gyrA*	C290T	S97L
60-r3	50	12.5	0.024	*gyrA*	C1052T	P342L
60-r4	>50	25	0.024	*gyrA*	C536T	A179V
60-r5	>50	25	0.024	*gyrA*	C536T	A179V
60-r6	>50	12.5	0.024	*gyrA*	C251T	A84V
60-r7	50	12.5	0.024	*gyrA*	A998G	N333S
60-r8	50	1.6	0.024	*gyrA*	T514G	S172A
60-r9	50	25	0.024	*gyrB*	C1367A	A456E

Figure 6.3 | Genome studies reveal DNA gyrase as a target. A) Agar containing **60** (5x MIC) was inoculated with 10^7 CFU of *E. coli*. After one day, nine viable colonies were isolated and used for MIC testing and whole-genome sequencing (WGS). **B)** Susceptibility assays confirm spontaneous resistance to **60** and WGS identified mutations located in the DNA gyrase, predominantly in subunit A. Cross-resistance is observed for conformationally restricted compound LEI-800. **C)** Topology of the mutations in the core of the DNA gyrase heterotetramer outline a possible binding site of isoquinoline sulfonamides. **D)** All mutations are found in the cleavage-reunion domain of DNA gyrase. Domain organization of DNA gyrase, GyrB (coral) and GyrA (beige) subunits.

Whole-genome sequencing of the strains showing resistance to compound **60** revealed that each had mutations in the gene encoding bacterial DNA gyrase (Figure 6.3B, Table S6.2), a heterotetrameric protein complex comprising two GyrA and two GyrB subunits. Eight of the colonies were found to contain mutations in GyrA, primarily in the N-terminal winged-helix (A84V, S97L) or the tower domains (S172A, A179V, N33S, P324L) (Figure 6.3C), and one in GyrB (A456E). Mapping these mutation sites on a recently published cryo-EM structural model of DNA gyrase[5] revealed their spatial proximity and suggested a potential binding pocket (Figure 6.3D).

To validate that these mutations in *gyrA* were indeed responsible for the resistance towards **60**, a CRISPR/Cas9 system was used to introduce the highly resistant *gyrA* S97L mutation, found in mutants **60**-r1 and **60**-r2 (Figure 6.3B) in an *E. coli* wild type background. It was confirmed that bacteria containing the S97L mutation were resistant against compounds **60**

and LEI-800 (Table S6.4). This combined with the whole-genome sequencing results strongly suggests that DNA gyrase is the primary target of the isoquinoline sulfonamides.

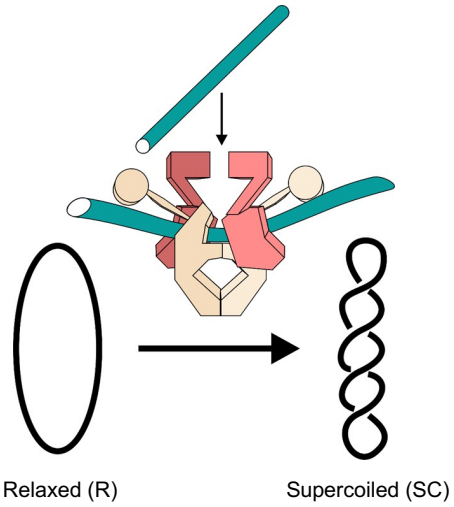

Figure 6.4 | Schematic representation of negative supercoiling. In a supercoiling assay, relaxed (R) DNA is transformed into supercoiled (SC) DNA by DNA gyrase.

LEI-800 is a highly potent DNA gyrase supercoiling inhibitor. DNA gyrase is a well-validated antibiotic target, which is responsible for introducing negative supercoils in DNA (Figure 6.4), a process that is required for DNA synthesis and proliferation of bacteria. DNA gyrase is a target of the fluoroquinolone antibiotics including CIP. To test whether LEI-800 was able to directly interact with DNA gyrase, LEI-800 was incubated in a concentration-dependent manner with recombinant *E. coli* DNA gyrase and its supercoiling activity was measured in a gel-based assay (Figure 6.5A,B). The activity of LEI-800 was compared to inactive control LEI-801. CIP was taken along as a positive control and produced an IC_{50} value of 925 nM, which is in line with previously reported values.[6] Remarkably, LEI-800 inhibited DNA gyrase activity with an IC_{50} of 35 nM, thereby making it >25-fold more potent than CIP. Mirroring the phenotypic screening results, control compound LEI-801 was 13-fold less potent than LEI-800, thereby confirming that the *cis-2R,5R* isomer is the distomer. Taken together, these biochemical studies demonstrate that the isoquinoline sulfonamides are potent inhibitors of DNA gyrase.

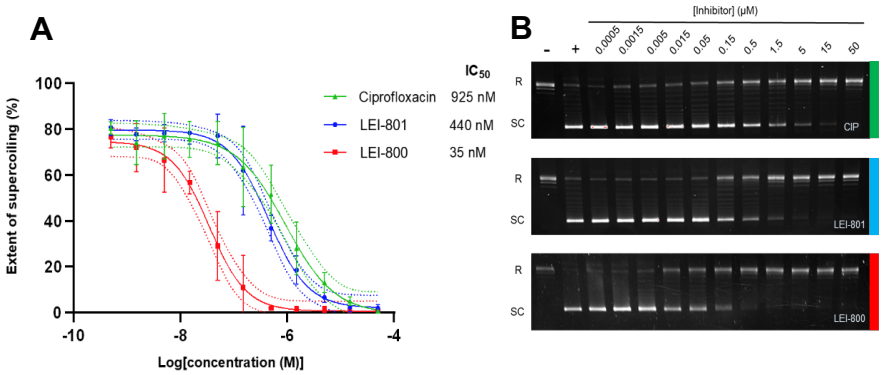

Figure 6.5 | LEI-800 is an exceptionally strong supercoiling inhibitor. A) Dose-response curves of DNA gyrase supercoiling inhibition, based on n = 3 gels. Error bars and dotted lines represent the standard deviation at each concentration and the 95% CI respectively. **B)** Representative agarose gels for *E. coli* DNA gyrase supercoiling inhibition by the three compounds.

Cellular penetration limits activity of LEI-800. The biochemical data showed that LEI-800 is a nanomolar range inhibitor of DNA gyrase, but its antimicrobial activity is in the low micromolar range (Table 6.1). It was hypothesized that this discrepancy could be due to active efflux by TolC, a major bacterial transporter or poor cellular uptake caused by the Gram-negative OM.[7] To distinguish between these possibilities, it was first checked whether LEI-800 and LEI-801 showed enhanced potency in the Δ*tolC* efflux pump mutant. No increase in potency was observed, suggesting that the isoquinoline sulfonamides are not substrates of the TolC efflux pump. Next, LEI-800 and LEI-801 were tested on *E. coli* strains containing loss-of-function mutations to outer membrane lipopolysaccharide (LPS) assembly genes (Δ*rfaC*, Δ*rfaY*, Δ*rfaI*, Δ*rfaP* and Δ*rfaD*) (Table S6.5). While the LPS biosynthesis mutations did not lead to an increase in activity of CIP, the antibacterial effect of LEI-800 was strongly potentiated in all mutants. Of note, the activity of LEI-801 was also potentiated in the Δ*rfaC*, Δ*rfaP* and Δ*rfaD* strains.

Table 6.1 | Supercoiling inhibition alongside antimicrobial activity in WT *E. coli* and in genetic and pharmacological LPS disruption backgrounds.

	IC_{50} (95% CI) (nM)	MIC (μM)		
		E. coli	*E. coli* ΔrfaC	*E. coli* + 8 μM PMBN
	supercoiling inhibition	WT strain	LPS disruption (genetic)	LPS disruption (pharmacological)
CIP	925 (553 – 1828)	0.024	0.024	0.024
LEI-801	440 (321– 624)	>50	3.1	6.25
LEI-800	35 (23 – 50)	3.1	0.4	0.4

A similar increase in sensitivity was observed when *E. coli* was co-treated with LEI-800 or LEI-801 in presence of polymyxin B nonapeptide (PMBN) (Table 6.1), a well-characterized[8] disrupting agent of the Gram-negative OM.[9] The synergistic effect of PMBN and the LEI compounds was further explored with a checkerboard assay (Figure 6.6). Clear synergy was seen for LEI-800 and LEI-801, while none was observed for CIP. The potentiating effect of PMBN on LEI-800 was maintained across the panel of clinical isolates tested (Table S6.6). Thus, both genetic and pharmacological studies indicate that the Gram-negative OM limits the cellular penetration of the isoquinoline sulfonamides.

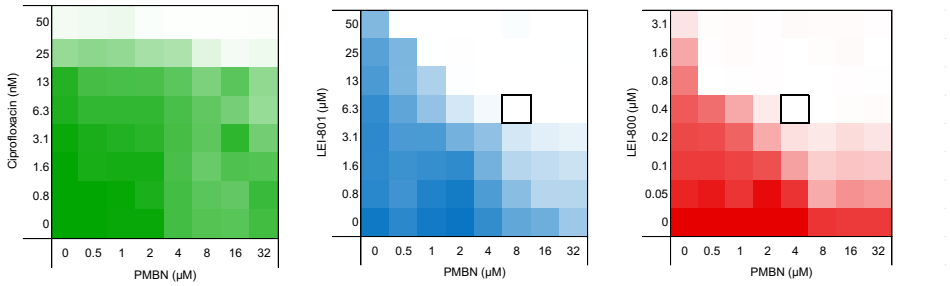

Figure 6.6 | Checkerboard assays show pharmacological disruption of LPS by PMBN does not have an effect on the antimicrobial activity of CIP, yet potentiates both LEI-801 and LEI-800.

Cryo-EM reveals unique binding pocket of LEI-800 within the DNA gyrase complex. To validate the presumed binding pocket of LEI-800 on the GyrA subunit, cryogenic electron microscopy (cryo-EM) was used to determine a medium-resolution structure of *E. coli* gyrase holocomplex (A_2B_2) bound to the substrate 217-bp dsDNA, nucleotide analogue ADPNP and LEI-800. A single dataset collected on 200 kV Glacios microscope allowed the visualization of the enzyme-DNA complex in the wrapped state (see Figure S6.1) and to reconstruct a model for the cleavage-reunion domain of the enzyme (residues 8-524 of GyrA and 405-804 of GyrB) similarly to Lamour and coworkers,[5] at the resolution of 4.2 Å (Figure 6.7A). CTDs of GyrA with wrapped DNA and ATPase domains of GyrB were also observed but not modelled**.** While the overall conformation of the complex was comparable to the available *E. coli* gyrase cryo-EM structure in complex with gepotidacin (PDB: 6RKW and 6RKV), there was a striking difference in the position of CTDs which were shifted upwards to form a narrow angle with the GyrB ATPase domains (Figure S6.1). The DNA substrate was seemingly intact, suggesting LEI-800, unlike fluoroquinolones, does not stabilize cleaved DNA complex.

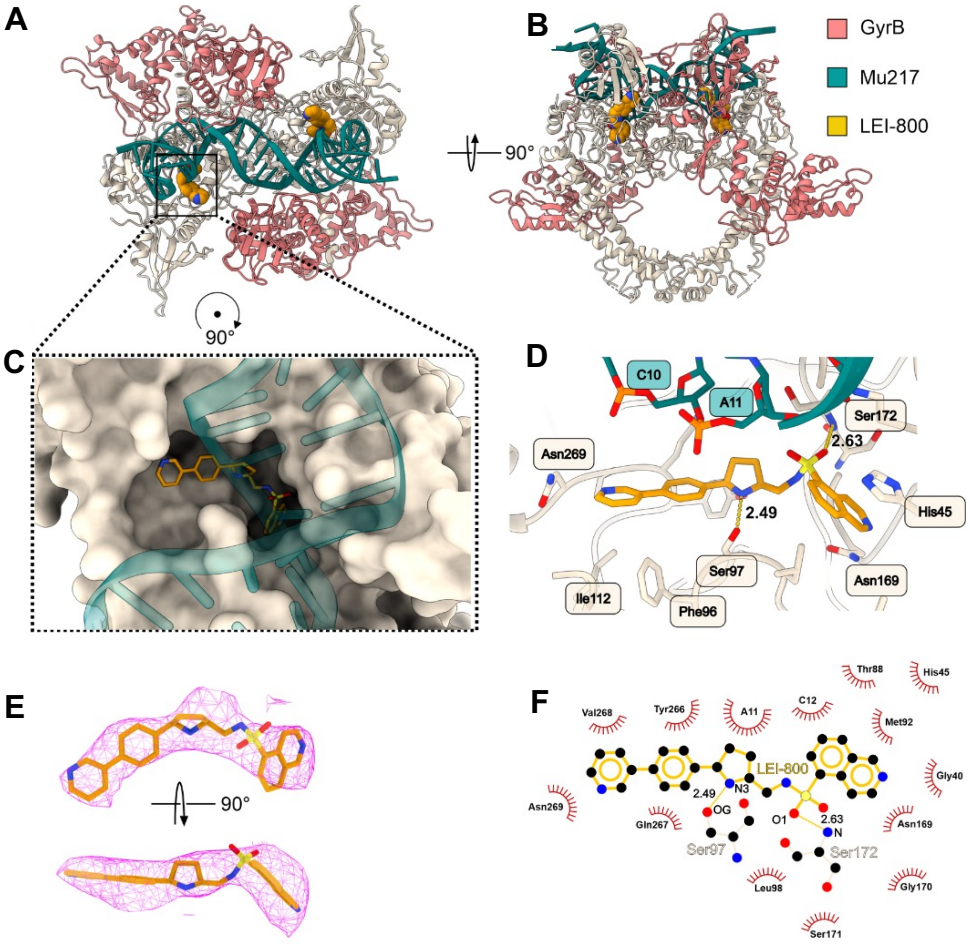

Figure 6.7 | Cryo-EM reveals unique binding pocket of LEI-800 within DNA gyrase. A,B) Overview of the model of the Gyr-Mu217-LEI-800 complex. GyrA (8-524) and GyrB (402-790) are depicted as beige and coral cartoon representations. The modelled central part of Mu217 DNA is shown in teal green. Two molecules of LEI-800 observed in a single gyrase heteroteramer are shown as golden van der Waals spheres. Uniform color scheme is used throughout the manuscript. **C)** A close-up of the LEI-800 binding pocket on the DNA-binding surface of GyrA. GyrA is shown as molecular surface, DNA as cartoon representation and LEI-800 as van der Waals spheres. **D)** Molecular interactions between GyrA and LEI-800. LEI-800 is shown as stick representation. Main GyrA residues important for LEI-800 binding are labelled. Two key hydrogen bonds between side-chain of Ser97 and N3 nitrogen of central pyrrolidine ring of LEI-800, and main chain nitrogen of Ser172 and sulfonic acid of LEI-800 are shown in gold; distances in Å are indicated. **E)** Coulomb potential density map for LEI-800. **F)** A 2D diagram of LEI-800 binding site generated by LigPlot. Key hydrogen bonds to Ser97 and Ser172 are shown in gold and distances in Å are indicated. Spiked red arcs show non-bonded interactions with residues within 3.9 Å distance.

Guided by mutations (Figure 6.3B), LEI-800 was easily identified as the distinct density, clearly separated from both DNA and protein (Figure 6.7A,E). One molecule of LEI-800 was bound to each GyrA subunit, occupying a horseshoe-like hydrophobic pocket on the DNA-binding surface (Figure 6.7C) just underneath the DNA but far away (>20 Å) from the catalytic residues. The curved shape of LEI-800 perfectly corresponded to the shape of the pocket, while the opposite would be the case for distomer LEI-801. The quinoline ring was lodged between His45 and Leu98 of GyrA while the pyridine ring is positioned right on top of the GyrA Ile112 and Phe96. Remarkably, two hydrogen bonds anchoring LEI-800 at place were made by the side chain of GyrA Ser97 (to the N3 of the central pyrrolidine ring) and the main chain of GyrA Ser172 (to the sulfonic acid moiety) (Figure 6.7D,F). Therefore, not only the main mutation (Ser97 to Ala) selected upon exposure to LEI-800 would clearly prevent the interaction, but also the initial SAR observation that nitrogen-containing linker is of crucial importance is now fully substantiated. Similarly, side-chain interaction with Ser172 explains how S172A mutation can slightly potentiate LEI-800 activity.

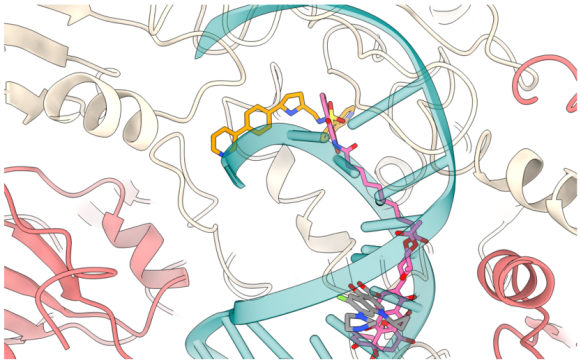

Figure 6.8 | A comparison of LEI-800 (current study), ciprofloxacin (CIP) (PDB:2XCT) simocyclinone D8 (SD8) (PDB:4CKL) binding sites on GyrA DNA-binding surface. LEI-800 is shown as golden, SD8 as pink and CIP as grey stick representations. A quinoline ring of LEI-800 shares binding pocket with the aminocoumarin moiety of SD8, but unlike SD8, LEI-800 does not interfere with DNA binding.

The LEI-800 pocket is not exploited by any type of natural or synthetic gyrase inhibitors and therefore presents an exciting opportunity for the development of a new class of drugs unaffected by the existing fluoroquinolone or "novel bacterial topoisomerase inhibitors" (NBTI) resistance. The only inhibitor bound in the partially overlapping site is simocyclinone D8 (SD8), a natural product preventing DNA binding to the GyrA subunit (Figure 6.8). In contrast to the SD8, LEI-800 binding seems not to affect interaction with DNA and therefore, it has to be concluded that LEI-800 inhibits gyrase by an unknown allosteric mechanism, detailed investigation of which remains out of scope of the current study.

LEI-800 shows activity against fluoroquinolone-resistant clinical isolates. With structural evidence supporting a unique binding mode for LEI-800 relative to known gyrase inhibitors, it was hypothesized that LEI-800 would be active against fluoroquinolone-resistant strains. First it was queried whether there is cross-resistance between LEI-800 and CIP, by testing strains with point mutations that confer resistance against one of the drugs. CIP was still fully active against all the isoquinoline resistant strains generated earlier in this study (Figure 6.3B). At the same time, introduction of single mutations in *gyrA* that confer fluoroquinolone resistance (specifically S83L[10,11] and D87N[10]) resulted in at least 60-fold increase in the MIC of CIP, but did not affect the susceptibility to LEI-800 (Table S6.4).

Table 6.2 | Antibacterial activity of LEI-800 against fluoroquinolone- resistant clinical isolates of *E. coli*

Clinical Isolates[a]		LEI-800	LEI-800 +PMBN		CIP	CIP +PMBN
ID	Resistance	MIC	MSC	FC	MSC	MSC
965	MDR	12.5	0.8	16	1	1
991		25	3.1	8	>32	>32
1022	ESBL	25	1.6	16	>32	>32
1104	MDR	25	1.6	16	>32	>32
1146	MDR	6.25	0.8	8	>32	>32
1175	MDR	25	3.1	8	>32	>32
1192	MDR	50	3.1	16	>32	>32
1201	MDR	12.5	1.6	8	>32	>32
1233		12.5	1.6	8	>32	>32

[a]*E. coli* Isolated from blood cultures and positive for CIP resistance. PMBN: polymyxin B nonapeptide, MIC: minimum inhibitory concentration, MSC: minimum synergistic concentration with 4 μM PMBN, FC: fold-change in MIC, MDR: multidrug resistant, ESBL extended spectrum beta lactamase producing.

Furthermore, 12 clinical strains with high reported resistance against fluoroquinolones were obtained and tested revealing that LEI-800 indeed exhibited antibacterial activity against all of them (Table 6.2). As with the other strains tested, the addition of PMBN resulted in strong potentiation of the antibacterial activity of LEI-800 against the highly CIP resistant isolates. Taken together, these data show that isoquinoline sulfonamides are a new class of antibiotics that target DNA gyrase in fluoroquinolone-resistant bacteria.

Discussion

For decades, the bacterial DNA gyrase has proven to be an excellent target for antibiotics with a number of clinically used anti-infectives operating by inhibiting its activty.[12] Given that DNA gyrase lacks a direct human homolog, has multiple target sites, and is essential to bacterial DNA function, inhibitors have the potential to selectively target bacterial cells vs host cells. Notably, the DNA supercoiling activity of DNA gyrase is a multi-step process that can be interrupted at multiple stages through pharmacological intervention.[13] Key examples being the classical fluoroquinolone antibiotics[14] and the more recent "novel bacterial type II topoisomerase inhibitors" (NBTIs)[15] that intercalate in DNA, the aminocoumarins[16] that compete with ATP, and SD8[17] that prevents DNA binding. Despite successful clinical application, resistance to fluoroquinolones is increasingly abundant[18,19] and the mammalian toxicity of fluoroquinolones,[20] NBTIs[21] and aminocoumarins present serious clinical concerns. In this light there is a clear need and opportunity for the development of improved next-generation DNA gyrase inhibitors.

Here, an entirely novel class of DNA gyrase inhibitors termed the isoquinoline sulfonamides is disclosed. Initially found through phenotypic screening of an existing compound set, extensive SAR studies led to the identification of key isoquinoline sulfonamide pharmacophores required for *in vitro* activity against *E. coli* and *K. pneumoniae*, after which conformational restriction of the initial scaffold led to the lead compound LEI-800**.** LEI-800 exhibits potent, Gram-negative-specific antibacterial activity with little mammalian cell toxicity. Cell morphology and mutation selection clearly pointed to DNA gyrase as the target for LEI-800 after which a cryo-EM study revealed that the compound binds to a previously unexploited site on the GyrA subunit. Somewhat surprisingly, LEI-800 shows no affinity for binding to DNA, as is common in other DNA gyrase inhibitors. In addition, the specific antibacterial activity of LEI-800 against *E. coli* and *K. pneumoniae* but not towards other bacterial pathogens may be explained by the low homology of the *E. coli* DNA gyrase (Table S6.7).

When directly compared to the clinically used fluoroquinolone CIP**,** LEI-800 was found to exhibit a number of key differences: 1) morphological studies with bacterial cytological profiling indicated that *E. coli* cells respond differently to CIP treatment than to LEI-800; 2) no significant cross-resistance was found between CIP and LEI-800 in strains harboring resistance-inducing point mutations, further highlighted by the susceptibility of CIP resistant clinical isolates to LEI-800; and 3) structural insights derived from cryo-EM studies reveal no overlap in the binding site of LEI-800 in the DNA gyrase compared with that of CIP. Based on this evidence, it was concluded that LEI-800 disrupts DNA gyrase activity via a novel MoA that is distinct from that of the fluoroquinolones. While CIP was found to generally exhibit lower MIC values than LEI-800 against fluoroquinolone-susceptible strains, it is interesting to note that LEI-800 is a much more potent inhibitor of DNA gyrase supercoiling activity *in vitro*, an effect most likely ascribed to the Gram-negative OM. Indeed, synergy assays with PMBN indicate that once past the OM, the antibacterial activity of LEI-800 is significantly

enhanced. This points to the potential for developing analogues of LEI-800 with improved OM permeability. In addition, the structural insights obtained for the interaction of LEI-800 with DNA gyrase provides a blueprint for the design of next generation inhibitors that might show enhanced resilience to resistance development.

To this end, future studies will be aimed at assessing the potential for inhibitors capable of simultaneously engaging with the distinct binding sights of CIP and LEI-800 to delay the emergence of resistance, the results of which will be reported in due course. In summary, LEI-800 belongs to a novel class of antibacterial agents with potent activity against Gram-negative bacteria, including clinical isolates, and binds to a unique pocket of DNA gyrase that is not exploited by other inhibitors of this key antibiotic target.

Acknowledgments

The following people are kindly acknowledged for their contribution to this chapter. Jeroen Punt for assisting with the synthesis, for setting up the bacterial cytological profiling assay, and for helping with the biochemical DNA gyrase assays. Mariana Avalos is thanked for generation and whole-genome profiling of the resistant mutants, and for the gene editing studies. Ioli Kotsogianni is thanked for assisting with the antibacterial assays. Jaco Slingerland is acknowledged for the synergy studies. Dmitry Ghilarov is thanked for the structure elucidation studies of LEI-800 with the DNA gyrase.

Methods

Reagents & materials. Buffers and salts were of ACS reagent grade or higher and were purchased commercially from Carl Roth GmbH (Karlsruhe, Germany) and Sigma-Aldrich (Darmstadt, Germany), biological materials and growth media were purchased from Sigma-Aldrich, Scharlab S.L. (Barcelona, Spain) and Fischer Scientific (Landsmeer, Netherlands). Antibiotics trimethoprim (Sigma-Aldrich), ceftazidime (ceftazidime pentahydrate, Thermo Scientific, Landsmeer, Netherlands) and kanamycin (kanamycin monosulfate, MP biomedicals, Illkirch, France) were dissolved in DMSO stored in -20ºC, apart from ciprofloxacin, which was used from a 3M aqueous solution containing 0.01% AcOH. All test compounds were used from 10 mM DMSO stock solutions made from the freeze-dried powder and stored at -20ºC.

Bacterial strains. *Klebsiella pneumoniae* ATCC 29665 (NCTC 11228), *Escherichia coli* ATCC 25922, *Pseudomonas aeruginosa* ATCC 27853, *Acinetobacter baumannii* ATCC BAA747 and *Staphylococcus aureus* USA300 (ATCC BAA1717) belong to the American Type Culture Collection (ATCC). *E. coli* NCTC 13463 and 13846 belong to the National Collection of Type Cultures (UK Health Security Agency). *E. coli* JW5503, JW3600, JW3602, JW3605 JW3594, JW3596 belong to the Keio Collection[22] of single-gene knockouts. *E. coli* NCTC 13463 and 13846 belong to the National Collection of Type Cultures (NCTC, UK Health Security Agency). *E. coli* strains 552059.1 and 552060.1 were isolated from urine[23] and acquired from the clinical Medical Microbiology department at the University Medical Center Utrecht. *E. coli* mcr-1 (EQAS 2016 412016126, mcr-1 positive, recovered during international antimicrobial resistance programs), W3110, BW25113, belong to the laboratory collection of prof. Nathaniel I. Martin. Fluoroquinolone resistant *E. coli* strains 965, 991, 1022, 1075, 1104,1146, 1175, 1192, 1201, 1233 were isolated from blood cultures, positive ciprofloxacin resistance, during July-August 2021 and were acquired from the Department of Medical Microbiology and Infection Prevention, Amsterdam University Medical Centre. The following reagents were obtained through BEI Resources, NIAID, NIH: *E. coli*, Strain MVAST0072, NR-51488.

Minimum inhibitory concentration. MIC was determined by broth microdilution. Single colony cultures were grown to exponential phase (OD600: 0.5) aerobically at 37°C. In case of strains from the Keio collection[22], 50 μg/mL kanamycin was supplemented to the media to ascertain a homogeneous population. The bacterial suspensions were diluted 100-fold in CAMHB and 50 μL was added to a 2-fold serial dilution series of test compounds (50 μL per well) in polypropylene 96-well microtiter plates to reach a volume of 100 μL. The plates were sealed with breathable membranes and incubated overnight at 37°C with constant shaking (600 rpm). The MIC was determined as the lowest concentration at which no visible bacterial growth was observed, as compared to the inoculum controls, from the median of a minimum of triplicates.

Bacterial cytological profiling. Overnight *E. coli* BW25113 cultures were diluted 1:100 in fresh LB medium in a 100 mL Erlenmeyer flask and incubated at 120 rpm and 37°C. When OD600 > 0.2, the cultures were diluted to OD600 = 0.1 in fresh LB medium with a final volume of 200 μL in a 2 mL Eppendorf tube. The appropriate antibiotic or control treatment was applied and the samples were incubated at 200 rpm and 30°C for 2 h. Subsequently, DAPI (2 μg/mL), FM4-64 (2 μg/mL) and SYTOX Green (0.5 μM) were added to reach the desired concentration and the samples were incubated a further 10 min. The samples were then centrifuged at 3300 × g for 50 s and the pellets resuspended in half the original volume. From this suspension, 5 μL was spotted onto a 2.0% agarose pad for microscopy.

Microscopy was performed on a Zeiss Axio Observer Z1/7 inverted microscope. For differential interference contrast the transmitted light source was an Aquilla TL halogen lamp (3.0 V). For widefield fluorescence the Zeiss Colibri.2 LED lamps were configured as follows: DAPI (365 nm, 150 ms, 25.42%), FM4-64 (590 nm, 1000 ms, 100%) and SYTOX Green (470 nm, 150 ms, 25.42%). Illuminated and reflected light were led through the following filters: DAPI (Zeiss 49: excitation = G 365, beam splitter = FT 395, emission = BP 445/50), FM4-64 (Zeiss 63: excitation = BP 572/25 (HE), beam splitter = FT 590 (HE), emission = BP 629/62 (HE)) and SytoxGreen (Zeiss 38: excitation = BP 470/40 (HE), beam splitter

= FT 495 (HE), emission = BP 525/50 (HE)). Images were collected through a Plan-Apochromat 100×/1.40 objective in oil immersion (n = 1.518) with a Hamamatsu C9100-02 camera.

Specific information on the programs and parameters used during image analysis are displayed in Table S6.6. For the qualitative assessment of the bacterial morphology, the acquired images were first pre-processed in ImageJ (v 1.53m). Thereafter the brightness and contrast were adjusted to allow the clearest visual inspection of the particular phenotype. For the quantitative BCP, DIC images were first pre-processed and then a random forest classifier was trained with Illastik (v 1.3.3) to generate a segmented image. These binary masks were then combined together with the original DIC image and processed with the ImageJ plugin MicrobeJ (v 5.13l). MicrobeJ generated cell outlines and performed measurements on cell shape accordingly. The recorded cell outlines produced by MicrobeJ were exported and used as a guide to characterize the DNA shape within each bacterium using a custom-made ImageJ macro (Appendix II). DAPI and SYTOX Green intensity were measured on raw images in a similar manner. Then by hand polygons were drawn that excluded bacteria to determine background intensity. After background correction the intensity was standardized to the DMSO control within the same biological replicate. For principal component analysis, the BCP assay was executed for three independently biological replicates. During each experiment, images were acquired until 30 or more bacteria in total had been observed. Following feature extraction for each replicate, principal component analysis was performed using GraphPad Prism (v 9.0.0) using multiple variable analysis with standardized data. PCs were selected based on the percent of total explained variance (minimum 80%).

Resistant mutant generation. Spontaneous resistant colonies were obtained by plating 100 µL of *E. coli* inoculum grown to an O.D. of 0.5 (~10^7 CFU) onto LB agar plates containing 5x the MIC of compound 60. The plates were incubated at 37°C and checked for growth after 24 and 48 h. Single colonies were picked after 48 h of incubation and their MIC was determined as described previously. Nine colonies with an increased MIC were selected for further analysis and stored as glycerol stocks.

Whole-genome sequencing. Nine spontaneous **60**-resistant mutants of *E. coli* were selected for genome sequencing. DNA was extracted as described elsewhere.[24] Briefly, *E. coli* cells were harvested from an overnight culture and re-suspended in lysis buffer (TE, SDS 10%, proteinase K), incubated for 1 h at 37°C. classical extraction with phenol-chloroform was performed and the aqueous layer was precipitated with absolute ethanol. The DNA pellet was washed with 70% ethanol, dried and solubilized in TE to perform RNA digestion with RNase 50 µg/mL (RNase A, Thermo Fischer). Degraded RNA was removed by phenol/chloroform extraction followed by ethanol precipitation. DNA was re-suspended in nuclease-free water. Genome sequencing was performed using Illumina Novaseq 6000 PE150 at Novogene. Paired-end sequence reads were generated and mapped against the reference genome of *E. coli* W3110. The alignment to the reference genome was performed using the Burrow-Wheeler Alignment tool (BWA v0.7.8[25]). SNP/InDel calling, annotation and statistics was performed using SAMtools[26] (v0.1.19) and ANNOVAR[27] (v2015MAR22). The structural variant calling annotation and statistics was performed with BreakDancer v1.4.4 and ANNOVAR[27] (v2015MAR22). The wild type *E. coli* W3110 was also sequenced and compared to the reference genome to confirm that the mutations found in the 60-resistant colonies were unique and related to the antibiotic resistance.

Construction of *gyrA* recombinant mutants in *E. coli* W3110. Mutants of the DNA gyrase subunit A encoding gene (*gyrA*) were constructed following the protocol for gene editing via the CRISPR-Cas9 system.[28] Strains and plasmids used are listed in Table S6.8 and primers used can be found in Table S6.9. The following mutations were created: S97L in *E. coli* W3110. Two common mutations in the *gyrA* gene that give resistance to fluoroquinolone antibiotics were created in *E. coli* W3110, namely S83L and D87N. To create the *gyrA* [S97L] mutants, the construct psgRNA-gyrA-M5 was assembled as follows: The 20 nt spacer sequence was introduced by PCR on pTargetF using primers gyrA_P11 and gyrA_P12, the homology-directed repair arms were amplified from *E. coli* W3110 genomic DNA by PCR using primer pairs gyrA_P05 and gyrA_P013, and gyrA_P08 and gyrA_P14. The three PCR fragments generated were cloned into the SpeI and BglII digested pTargetF via Gibson assembly. To avoid off-target effects of CRISPR, besides desired point mutation for *gyrA*[S97L], four other silent point mutations were also included in HDR template. Consequently, the amino acid sequence of *gyrA* will

remain the same in the generated mutant except for the desired mutation. Similarly, constructs psgRNA-gyrA-S83L *and* psgRNA-gyrA-D87N were created to introduce mutations S83L and D87N in *gyrA*, respectively. In psgRNA-gyrA-S83L, spacer sequence was introduced using primers gyrA_P12 and gyrA_P17, HDR template was amplified using primer pairs gyrA_P05 and gyrA_P18, and gyrA_P08 and gyrA_P19. In psgRNA-gyrA-D87N, spacer sequence was introduced using primers gyrA_P12 and gyrA_P20, HDR template was amplified using primer pairs gyrA_P05 and gyrA_P21, and gyrA_P08 and gyrA_P22. The verified constructs for *gyrA* engineering were transformed into *E. coli* W3110 carrying pCas9, and plated in LB containing kanamycin (50 μg/mL) for the selection of the pCas9 plasmid and spectinomycin (100 μg/mL) for the selection of psgRNA-gyrA-X. The plates were incubated at 30°C. Plasmids were cured by growing the strains with 0.5 mM IPTG and no antibiotics to lose first the psgRNA-gyrA plasmids. After losing the spectinomycin resistance, the strain was grown in LB with no antibiotics at 42°C to lose the pCas plasmid. Colony PCR was performed on plasmid-free colonies using primers gyrA_P9 and gyrA_P10, and PCR products were sequenced to confirm the desired mutation.

DNA gyrase supercoiling assay. The DNA gyrase inhibition assay was executed as instructed by the manufacturer (G1001 from Inspiralis Limited). A master mix was made including 0.5 μg relaxed plasmid (pBR322) in 35 mM Tris·HCl (pH 7.5), 24 mM KCl, 4 mM $MgCl_2$, 2 mM DTT, 1.8 mM spermidine, 1 mM ATP, 6.5% (w/v) glycerol, and 0.1 mg/mL albumin per reaction. Of this stock solution 27 μL was aliquoted for each reaction in 1.5 mL Eppendorf tubes and supplemented with 0.6 μL of the appropriate compound dilution or corresponding solvent with a final DMSO concentration of 2%. The reactions were started with 3 μL of enzyme (1 U) in dilution buffer (50 mM Tris·HCl (pH 7.5), 100 mM KCl, 2 mM DTT, 1 mM EDTA, and 50% (w/v) glycerol) for a final volume of 30 μL. Reactions were run at 37°C for 30 min and stopped with the addition of 30 μL Stop Dye (40% (w/v) sucrose, 100 mM Tris·HCl pH 8, 10 mM EDTA, 0.5 mg/mL Bromophenol Blue) and 30 μL of a chloroform:isoamyl alcohol solution (24:1 v/v). After brief vortexing and centrifugation at 2300 × g for 1 min, 20 μL of the aqueous phase was loaded onto a 1% (w/v) agarose gel in TAE (Tris·acetate 0.04 mM, EDTA 0.002 mM) gel. The gel was run at 85 V for 2 h followed by staining (15 min) in 1 μg/mL ethidium bromide and destaining (5-10 min) in water. DNA was visualized (602/50, UV Trans, auto optimal exposure) with a ChemiDoc MP (Bio-Rad Laboratories, Inc) and the percentage of supercoiled DNA relative to the total amount material per lane was determined with ImageLab 6.1 software (Bio-Rad Laboratories, Inc). IC_{50} curves were generated in GraphPad Prism (v 9.0.0) using the nonlinear regression curve fit variable slope with four parameters and least squares regression.

Checkerboard assay. Dilution series of both the test compound and Polymyxin B Nonapeptide (PMBN) were prepared in CAMHB media. To evaluate synergy, 25 μL of test compound solutions were added to wells containing 25 μL of PMBN solution. This was replicated in three columns for each combination so as to obtain triplicates. 50 μL of bacterial stock was added, and the plates were sealed with breathable membranes. After incubation for 20 hours at 37°C while shaking at 600 rpm, the breathable seals were removed and the plates shaken using a bench top shaker to ensure homogeneous bacterial suspensions. The plates were then transferred to a Tecan Spark plate reader and following another brief shaking (20 seconds) the density of the bacterial suspensions measured at 600 nm (OD600). The resulting OD600 values were transformed to a 2D gradient to visualize the growth/no-growth results. (Table S6.10, and Synergy assay methods below for calculations of Fractional Inhibitory Concentration Index and synergy definitions).

Synergy assay: Fractional Inhibitory Concentration Index (FICI)

The FICI was calculated using Equation 1 where synergy is indicated by FICI ≤ 0.5.[29]

$$\mathbf{FICI} = \frac{\mathbf{MSC_{ant}}}{\mathbf{MIC_{ant}}} + \frac{\mathbf{MSC_{syn}}}{\mathbf{MIC_{syn}}} \quad (1)$$

Equation 1. Calculation of FICI. MSC_{ant} = MIC of antibiotic in combination with synergist; MIC_{ant} = MIC of antibiotic alone; MSC_{syn} = MIC of synergist in combination with antibiotic; MIC_{syn} = MIC of synergist alone. In cases where the MIC of the antibiotic or synergist was found to exceed the highest

concentration tested, the highest concentration in the dilution series was used in determining the FICI and the result reported as ≤ the calculated value.

Cryogenic electron microscopy sample preparation. Plasmids for the expression of *E. coli* GyrA and GyrB (pET28-GyrATS and pET28-GyrBTS) were previously described[5] and obtained as a gift of Prof. Valerie Lamour (IGBMC, University of Strasbourg). GyrA and GyrB were purified as described.[5] 217 bp DNA (a strong gyrase binding site of phage Mu) was used as a substrate to. *E. coli* GyrA and GyrB subunits were mixed in equimolar proportions to reconstitute the full DNA gyrase enzyme. 217 bp DNA was added to the complex in a 1:1 ratio to a final concentration of gyrase-DNA complex ~15 μM. The reconstituted complex was buffer exchanged using dialysis at 4°C overnight to cryo-EM buffer (25 mM Na-HEPES pH 8, 30 mM potassium acetate, 2.5 mM magnesium acetate, 0.5 mM TCEP). After buffer exchange, the sample was concentrated to ~30 μM. Sample was supplemented with 100 μM LEI-800 compound, 1 mM ADPNP and incubated for 30 min at 37°C. 8 mM CHAPSO was added, and sample was centrifuged (60 min at 21,000 x g) to remove potential aggregates.

Cryo-electron microscopy data collection and analysis. Aliquots of 4 μl of reconstituted complexes (~12 mg/ml) were applied to glow-discharged (Leica, 60 s/8 mA) Quantifoil holey carbon grids (R2/1, 300 copper mesh). After 30 s of incubation with 95% chamber humidity at 10°C, the grids were blotted for 6 s and plunge-frozen in liquid ethane using a Vitrobot mark IV (FEI).

Cryo-EM data were collected at the Polish national cryo-EM facility SOLARIS with a Titan Glacios microscope (Thermo Fisher Scientific) operated at 200 kV, and images (movie frames) were collected at the calibrated physical pixel size of 0.95 Å per pixel with a defocus range of −3 to −0.9 μm. The images were recorded in counting mode on a Falcon IV electron direct detector (Thermo) in EER format. A dose rate and exposure time was set to generate a total dose of ~40 electrons/Å^2. Statistics for cryo-EM data collection are listed in Table S6.11.

All processing was done in cryoSPARC 3.3.1.[30] 10,362 movies were dose weighted and motion and CTF corrected in patch mode. Particles were picked with cryoSPARC template picker and 2x2 binned particles (1,575,192) were subjected to several rounds of 2D classification. Cleaned particles representing holoenzyme with secondary structure elements visible (183,664) underwent two rounds of 3D classification with 2 classes (CS3 ab initio, 134,472 particles retained) and was refined to 4.1 Å resolution using non-uniform refinement procedure.[31] Particles were re-extracted as unbinned using updated coordinates. Further non-uniform refinement of this particle set with local CTF correction[32] resulted in a final map of estimated 4.23 Å global resolution and 3.7 Å local resolution around the drug binding site. Multiple attempts to improve the FSC and resolution by global and focussed classification in both cryoSPARC and Relion did not bring improvement or highlighted a particular source of heterogeneity in the dataset; therefore, we concluded that in this case the resolution was limited by the quality of the original sample. The 4.23 Å map displayed more visible side-chains and best local resolution for LEI-800 binding pocket and therefore was selected for final refinement.

Model building and refinement. The closest available structure of *E. coli* gyrase (PDB:6RKV[5]) was used as a starting point for model building. 6RKV model was rigid-body fitted in ChimeraX[33] and manually adjusted in Coot.[34] Real-space refinement was performed in phenix.refine[35] (using Ramachandran restrains and secondary structure restraints). The model and restraints for LEI-800 were obtained using Grade server (http://grade.globalphasing.org); LEI-800 was initially manually fitted into the density and refined in Phenix. The model was refined against the 4.23 Å map described above. MolProbity[36] was used to validate the structures. Statistics for the final model is reported in Table S6.11.

Supplementary information

Table S6.1 | Parameters used during image analysis

Software	Analysis	Parameters/Command
ImageJ[37] (v 1.53m)	Qualitative BCP – DAPI channel	run("Subtract Background...", "rolling=15"); run("Mean...", "radius=1");

	Qualitative BCP – FM4-64 channel	run("Subtract Background...", "rolling=5");
		run("Enhance Contrast...", "saturated=0.3");
		run("Mean...", "radius=1");

	Qualitative BCP – DIC channel	No preprocessing
	Quantitative BCP – DIC channel	run("Gaussian...", "radius=1.5");
	Quantitative BCP – DAPI shape descriptors	Custom made script (Figure S1)
	Quantitative BCP – DAPI and SYTOX Green intensity	Custom made script (Figure S2)
Illastik[38] (v 1.3.3)	DIC image segmentation	All features selected Classifier trained for label “cell” or “background”
MicrobeJ[39] (v 5.13l)	Quantitative BCP – DIC shapes	Image used for bacteria detection: DIC channel Segmentation based on: binary mask generated by Illastik. Bacteria detection = fit shape (rod shaped) Attributes: Area (1.5 – max); Length (1.5 – max); Width (0.5 – max); Circularity (0 – max) Enabled options: Exclude on Edges; Shape descriptors; Segmentation (default settings); Intensity; Shape; Profile (medial, default settings)

strain	sample	POS1	Gene	REF	ALT	SNP	Protein	Amino acid	Normal	Mutant	TYPE of MUTATION	QUAL	DP	Note
60-r1	1a	2343801	*gyrA*	G	A	C290T	DNA gyrase subunit A	97	S	L	nonsynonymous SNV	222	205	good quality and depth
60-r2	3a	2343801	*gyrA*	G	A	C290T	DNA gyrase subunit A	97	S	L	nonsynonymous SNV	222	205	good quality and depth
60-r3	4a	2343066	*gyrA*	G	A	C1052T	DNA gyrase subunit A	342	P	L	nonsynonymous SNV	222	166	good quality and depth
60-r4	5a	2343555	*gyrA*	G	A	C536T	DNA gyrase subunit A	179	A	V	nonsynonymous SNV	222	208	good quality and depth
60-r5	6a	2343555	*gyrA*	G	A	C536T	DNA gyrase subunit A	179	A	V	nonsynonymous SNV	222	213	good quality and depth
60-r6	7a	2343840	*gyrA*	G	A	C251T	DNA gyrase subunit A	84	A	V	nonsynonymous SNV	222	194	good quality and depth
60-r7	8a	2343093	*gyrA*	T	C	A998G	DNA gyrase subunit A	333	N	S	nonsynonymous SNV	222	187	good quality and depth
60-r8	9a	2343577	*gyrA*	A	C	T514G	DNA gyrase subunit A	172	S	A	nonsynonymous SNV	222	186	good quality and depth
60-r9	10a	3761662	*gyrB*	C	A	C1367A	DNA gyrase subunit B	456	A	E	nonsynonymous SNV	222	228	good quality and depth
60-r9	10a	1197893	*icd*	T	A	T1194A	NADP-dependent isocitrate dehydrogenase	398	D	E	nonsynonymous SNV	49.3	6	low quality, low depth
60-r3	4a	1197893	*icd*	T	A	T1194A	NADP-dependent isocitrate dehydrogenase	398	D	E	nonsynonymous SNV	73	9	low quality, low depth
60-r4	5a	1197893	*icd*	T	A	T1194A	NADP-dependent isocitrate dehydrogenase	398	D	E	nonsynonymous SNV	27	4	low quality, low depth
60-r5	6a	1197893	*icd*	T	A	T1194A	NADP-dependent isocitrate dehydrogenase	398	D	E	nonsynonymous SNV	15.1	5	low quality, low depth
60-r6	7a	1197893	*icd*	T	A	T1194A	NADP-dependent isocitrate dehydrogenase	398	D	E	nonsynonymous SNV	69.1	6	low quality, low depth
60-r7	8a	1197893	*icd*	T	A	T1194A	NADP-dependent isocitrate dehydrogenase	398	D	E	nonsynonymous SNV	37.5	5	low quality, low depth
60-r8	9a	1197893	*icd*	T	A	T1194A	NADP-dependent isocitrate dehydrogenase	398	D	E	nonsynonymous SNV	37	4	low quality, low depth
60-r2	3a	4645108	*yjjY*	T	A	T27A	Uncharacterized protein YjjY	9	L	L	synonymous SNV	3.52	127	low quality, synonymous

Table S6.2. Extended data of whole-genome sequencing results of *E. coli* W3110 mutants.

Table S6.3 | MIC of known antibiotics and compounds against selected 60-resistant (60-r) selected isolates of W3110.

Antibiotic	Mode-of-action	MIC µM *E. coli*			
		W3110	**60**-r1	**60**-r3	**60**-r6
60		6.25	>100	100	>100
LEI-800		3.1	>50	12.5	12.5
Imipenem	PBP - cell wall	0.375	0.75	0.375	0.375
Meropenem	PBP - cell wall	0.05	0.09	0.05	0.05
Ceftazidime	PBP - cell wall	0.75	0.375	0.75	0.75
Colistin	Outer membrane	0.19	0.375	0.375	0.19
Trimethoprim	Folic acid synthesis	0.375	0.375	0.18	0.375
Neomycin	Protein synthesis (30S)	1.5	0.75	1.5	0.75
Chloramphenicol	Protein synthesis (50S)	12.4	12.4	12.4	12.4
Ciprofloxacin	DNA replication	0.024	0.024	0.024	0.024

Table S6.4 | CRISPR-*gyrA* editing. Target validation by introduction of point mutations with CRISPR/Cas9 on an *E. coli* W3110 background. MIC values are in agreement with sequenced spontaneous mutants.

E. coli W3110		MIC (µM)		
Mutation	Note	**60**	LEI-800	CIP
WT	WT	6.25	3.1	0.024
S97L	LEI-800-resistant	>50	>50	0.024
S83L	FQ-resistant 1	25	6.25	>1.5
D87N	FQ-resistant 2	50	6.25	>1.5

Table S6.5 | MIC (µM) on *E. coli* strains of the Keio collection.

Strain	Deletion	CIP	LEI-801	LEI-800
BW25113	parent	0.024	>50	3.1
JW5503	ΔTolC	0.024	>50	3.1
JW3600	ΔrfaY	0.024	>50	1.6
JW3602	ΔrfaI	0.024	>50	1.6
JW3605	ΔrfaP	0.048	12.5	0.4
JW3594	ΔrfaD	>0.048	3.1	0.4
JW3596	ΔrfaC	0.024	3.1	0.4

Table S6.6 | MIC (μM) of selection of compounds against clinical isolates of *E. coli* and potentiation by addition of 4 μM PMBN.

E. coli strain	Resistance profile	LEI-800	LEI-800 + PMBN		CIP	CIP + PMBN
		MIC	MSC	FC	MIC	MSC
mcr-1	*MCR*	25	6.25	*4*	>32	>32
NCTC13463	*ESBL*	3.1	0.4	*8*	1	1
NCTC13846	*MDR (mcr-1)*	50	12.5	*4*	>32	>32
MVAST0072[#]	*MDR*	25	1.5	*16*	>32	>32
552059.1[#]		25	0.78	*32*	1	1
552060.1[#]		25	1.5	*16*	1	1
1075	*MDR*	>50	12.5	*>4*	0.13	0.13

PMBN: Polymyxin B nonapeptide, CIP: ciprofloxacin, FC: fold change in MIC after addition of 4 μM PMBN, MCR: mobile colistin resistance, MDR: multidrug resistant, ESBL: extended spectrum beta lactamase, [#] urinary tract infection isolates.

Table S6.7a | Homology DNA gyrase subunit A (*E. coli*).

Organism	Strain	Uniprot ID	Protein	Gene	Homology[a]
E. coli	K12	GYRA_ECOLI	DNA gyrase subunit A	gyrA	100%
K. pneumoniae	342	B5XNZ4_KLEP3	DNA gyrase subunit A	gyrA	92.0%
E. faecium	ATCC 700802	H7C793_ENTFA	DNA gyrase subunit A	gyrA	47.1%
S. aureus	-	GYRA_STAA3	DNA gyrase subunit A	gyrA	46.3%
A. baumannii	-	Q2FCU6_ACIBA	DNA gyrase subunit A	gyrA	59.5%
P. aeruginosa	ATCC 15692	GYRA_PSEAE	DNA gyrase subunit A	gyrA	63.0%
Homo sapiens		TOP2A_HUMAN	DNA topoisomerase 2-alpha	TOP2A	23.4%
Homo sapiens		TOP2B_HUMAN	DNA topoisomerase 2-beta	TOP2B	25.6%

[a]Calculated by Uniprot Align function

Table S6.7b | Homology DNA gyrase subunit B (*E. coli*).

Organism	Strain	Uniprot ID	Protein	Gene	Homology[a]
E. coli	K12	GYRA_ECOLI	DNA gyrase subunit B	gyrB	100%
K. pneumoniae	342	J2E0G5_KLEPN	DNA gyrase subunit B	gyrB	92.0%
E. faecium	ATCC 700802	Q93HU9_ENTFL	DNA gyrase subunit B	gyrB	44.0%
S. aureus	-	GYRB_STAA3	DNA gyrase subunit B	gyrB	43.6%
A. baumannii	-	GYRB_ACIBA	DNA gyrase subunit B	gyrB	35.7%
P. aeruginosa	ATCC 15692	GYRB_PSEAE	DNA gyrase subunit B	gyrB	68.2%
Homo sapiens		TOP2A_HUMAN	DNA topoisomerase 2-alpha	TOP2A	25.8%
Homo sapiens		TOP2B_HUMAN	DNA topoisomerase 2-beta	TOP2B	25.8%

[a]Calculated by Uniprot Align function

Table S6.8 | Strains and plasmids used for the construction of the *gyrA* mutants.

Plasmid	Characteristics	Source or reference
E. coli W3110	Wild type ($F^-\lambda^-$rph-1 IN(rrnD, rrnE))	
E. coli DH5α	fhuA2 Δ (argF-lacZ)U169 phoA glnV44 Φ80 Δ(lacZ)M15 gyrA96 recA1 relA1 endA1 thi-1 hsdR17	Meselson & Yuan, 1968
pCas	repA101(Ts), kan^r , P_{cas}-cas9, P_{araB}-Red, $lacI^q$, P_{trc}-sgRNA-pMB1; temperature-sensitive replication vector	Jiang et al, 2015
pTargetF	pMB1, *aadA*, sgRNA-fts	Jiang et al, 2015
psgRNA-gyrA-M5	Plasmid used to insert the S97L mutation in *gyrA*	This study
psgRNA-gyrA-S83L	Plasmid used to insert the S83L mutation in *gyrA*	This study
psgRNA-gyrA-D87N	Plasmid used to insert the D97N mutation in *gyrA*	This study

Table S6.9 | Primers used for the construction of the *gyrA* mutants.

Primers	Sequence (5' to 3')
gyrA_P05	TTCTCTAGAGTCGACCTGCAGGAAGTCCGGCCCCGGGATGTGT
gyrA_P08	TCGAGTAGGGATAACAGGGTAATATCTAGAGGTTTACCGGCGATTTTTCGGCATTCAT
gyrA_P09	ATCAGCCCTTCAATGCTGATG
gyrA_P10	TCCGTAATTGGCAAGACAAAC
gyrA_P11	CTCAGTCCTAGGTATAATACTAGTAGCATATAACGCAGCGAGAAGTTTTAGAGCTAGAAATAGCAAGTTA AAATAAG
gyrA_P12	CTGCAGGTCGACTCTAGAGAATTCAAAAAAAGCACCGACTC
gyrA_P13	TTTACTACGTTACATGCTGGTAGACGGTCAGGGTAACTTCG
gyrA_P14	CCAGCATGTAACGTAGTAAAAATGGCTGCGCCATGCGGACGATC
gyrA_P17	CTCAGTCCTAGGTATAATACTAGTCATAGACCGCCGAGTCACCAGTTTTAGAGCTAGAAATAGCAAGTTA AAATAAG
gyrA_P18	GGAGATCTGGCTGTTTATGACACGATCGTCCGCATGGCGCAG
gyrA_P19	GTCATAAACAGCCAGATCTCCATGGGGATGGTATTTACCGATTACGTCACCAACGAC
gyrA_P20	CTCAGTCCTAGGTATAATACTAGCTATGACACGATCGTCCGCAGTTTTAGAGCTAGAAATAGCAAGTTAA AATAAG
gyrA_P21	CTATAACACAATAGTAAGGATGGCGCAGCCATTCTCGCTGCG
gyrA_P22	GCCATCCTTACTATTGTGTTATAGACCGCCGAGTCACCATGGGGATGG

Table S6.10 | Result table from checkerboard assays of antibiotics and PMBN as synergist on *E. coli* W3110.

	MSC	MIC	FICI (PMBN MIC>32)
Ciprofloxacin	0.025	0.05	1.5-2
LEI-801	6.25	200	≤0.28
LEI-800	0.39	3.13	≤0.25

MSC: minimum synergistic concentration, MIC minimum inhibitory concentration, FICI: Fractional Inhibitory Concentration Index, PMBN: Polymyxin B nonapeptide.

Table S6.11 | Data collection and refinement statistics.

Data collection and processing	EcGyr-Mu217-LEI-800
Microscope	ThermoFisher Glacios
Magnification	45000×
Voltage (kV)	300
Electron dose (e^-/Å^2)	39.91
Detector	Falcon 4
Defocus range (-μm)	3-0.9
Pixel size (Å)	0.95
Symmetry imposed	C1
Micrographs (no.)	10362
Initial particle images (no.)	1575192
Final particle images (no.)	132680
Global map resolution (Å)	4.23
FSC threshold	0.143
Refinement	
Model resolution (Å)	4.17
FSC threshold	0.143
Map sharpening *B* factor (Å^2)	129.4
Model composition	
Non-hydrogen atoms Protein residues	15278
Nucleotides	1784
Ligands	52
	2
Mean B factors (Å^2)	
Protein	60.74
Nucleotide	75.47
Ligands	19.30
R.m.s. deviations	
Bond lengths (Å)	0.004
Bond angles (°)	0.890
Validation	
MolProbity score	2.67
Clashscore	5.61
Ramachandran plot Favored (%)	
Allowed (%)	87.76
Disallowed (%)	11.00
	1.25

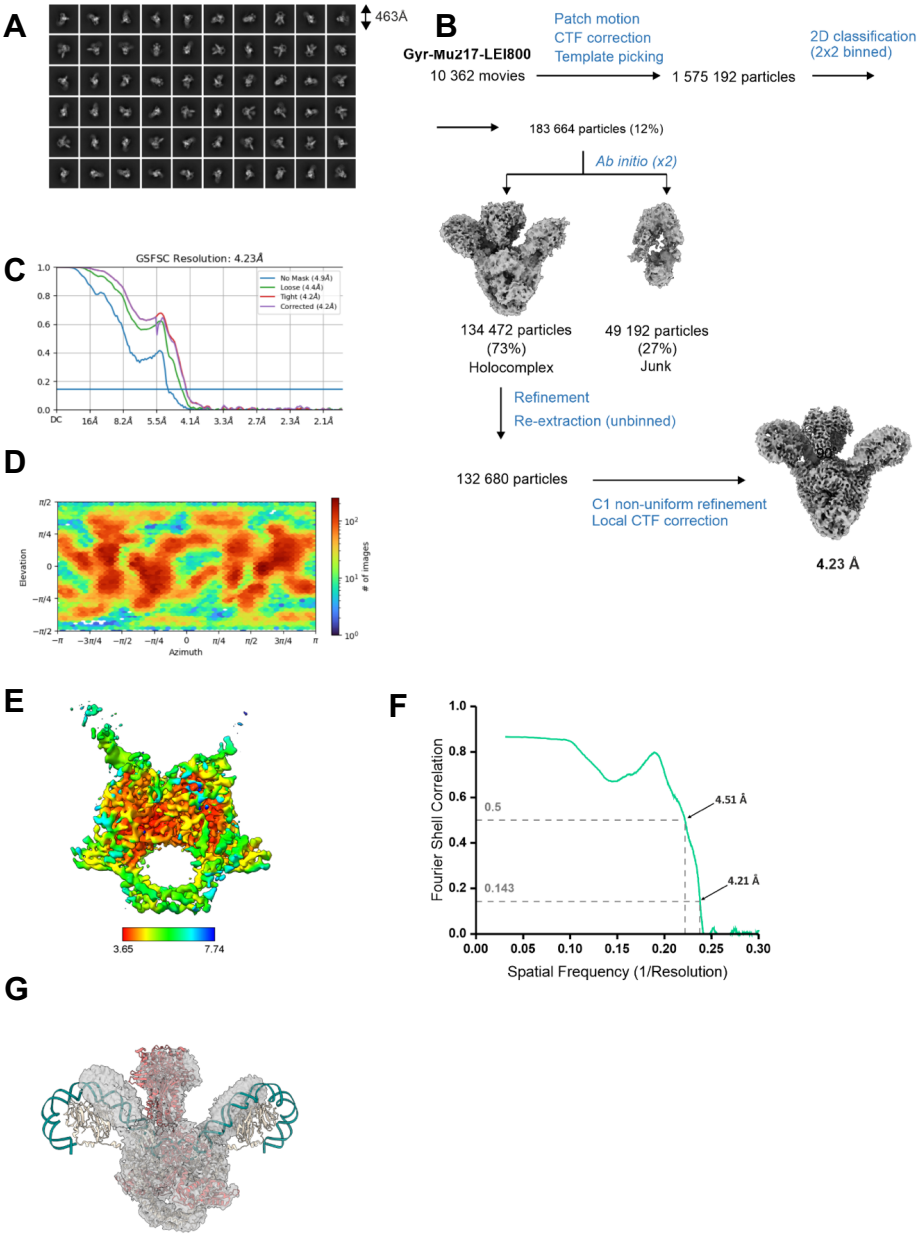

Figure S6.1 | Cryo-EM data processing for Gyr-Mu217-LEI-800. A) A selection of 2D classes, box size in Å indicated. **B)** Processing scheme (see Methods for description). **C)** FSC curve for the final reconstruction as output by cryoSPARC. **D)** Euler angle distribution as output by cryoSPARC. **E)** Local resolution map to illustrate resolution distribution from <4 Å next to the DNA and compound to >7 at the ends of the cleavage-reunion domain. **F)** Map-to-model curve. **G)** Comparison of Gyr-Mu217-LEI-800 map (grey surface) to the gepotidacin EM structure 6RKW (cartoon model). Note the significant change in the position of the CTDs and DNA.

References

(1) Asokan, G. V.; Ramadhan, T.; Ahmed, E.; Sanad, H. WHO Global Priority Pathogens List: A Bibliometric Analysis of Medline-Pubmed for Knowledge Mobilization to Infection Prevention and Control Practices in Bahrain. *Oman Med. J.* 2019, *34*, 184–193.

(2) Lewis, K. The Science of Antibiotic Discovery. *Cell* 2020, *181*, 29–45.

(3) Tacconelli, E.; Carrara, E.; Savoldi, A.; Harbarth, S.; Mendelson, M.; Monnet, D. L.; Pulcini, C.; Kahlmeter, G.; Kluytmans, J.; Carmeli, Y.; Ouellette, M.; Outterson, K.; Patel, J.; Cavaleri, M.; Cox, E. M.; Houchens, C. R.; Grayson, M. L.; Hansen, P.; Singh, N.; Theuretzbacher, U.; Magrini, N.; Aboderin, A. O.; Al-Abri, S. S.; Awang Jalil, N.; Benzonana, N.; Bhattacharya, S.; Brink, A. J.; Burkert, F. R.; Cars, O.; Cornaglia, G.; Dyar, O. J.; Friedrich, A. W.; Gales, A. C.; Gandra, S.; Giske, C. G.; Goff, D. A.; Goossens, H.; Gottlieb, T.; Guzman Blanco, M.; Hryniewicz, W.; Kattula, D.; Jinks, T.; Kanj, S. S.; Kerr, L.; Kieny, M. P.; Kim, Y. S.; Kozlov, R. S.; Labarca, J.; Laxminarayan, R.; Leder, K.; Leibovici, L.; Levy-Hara, G.; Littman, J.; Malhotra-Kumar, S.; Manchanda, V.; Moja, L.; Ndoye, B.; Pan, A.; Paterson, D. L.; Paul, M.; Qiu, H.; Ramon-Pardo, P.; Rodríguez-Baño, J.; Sanguinetti, M.; Sengupta, S.; Sharland, M.; Si-Mehand, M.; Silver, L. L.; Song, W.; Steinbakk, M.; Thomsen, J.; Thwaites, G. E.; van der Meer, J. W.; Van Kinh, N.; Vega, S.; Villegas, M. V.; Wechsler-Fördös, A.; Wertheim, H. F. L.; Wesangula, E.; Woodford, N.; Yilmaz, F. O.; Zorzet, A. Discovery, Research, and Development of New Antibiotics: The WHO Priority List of Antibiotic-Resistant Bacteria and Tuberculosis. *Lancet Infect. Dis.* 2018, *18*, 318–327.

(4) Nonejuie, P.; Burkart, M.; Pogliano, K.; Pogliano, J. Bacterial Cytological Profiling Rapidly Identifies the Cellular Pathways Targeted by Antibacterial Molecules. *Proc. Natl. Acad. Sci. U. S. A.* 2013, *110*, 16169–16174.

(5) Vanden Broeck, A.; Lotz, C.; Ortiz, J.; Lamour, V. Cryo-EM Structure of the Complete E. Coli DNA Gyrase Nucleoprotein Complex. *Nat. Commun.* 2019, *10*, 1–12.

(6) Chan, P. F.; Germe, T.; Bax, B. D.; Huang, J.; Thalji, R. K.; Bacqué, E.; Checchia, A.; Chen, D.; Cui, H.; DIng, X.; Ingraham, K.; McCloskey, L.; Raha, K.; Srikannathasan, V.; Maxwell, A.; Stavenger, R. A. Thiophene Antibacterials That Allosterically Stabilize DNA-Cleavage Complexes with DNA Gyrase. *Proc. Natl. Acad. Sci. U. S. A.* 2017, *114*, E4492–E4500.

(7) Masi, M.; Réfregiers, M.; Pos, K. M.; Pagès, J. M. Mechanisms of Envelope Permeability and Antibiotic Influx and Efflux in Gram-Negative Bacteria. *Nat. Microbiol.* 2017, *2*.

(8) Vaara, M. Agents That Increase the Permeability of the Outer Membrane. *Microbiol. Rev.* 1992, *56*, 395–411.

(9) Vaara, M.; Vaara, T. Sensitization of Gram-Negative Bacteria to Antibiotics and Complement by a Nontoxic Oligopeptide. *Nature* 1983, *303*, 526–528.

(10) Bhatnagar, K.; Wong, A. The Mutational Landscape of Quinolone Resistance in Escherichia Coli. *PLoS One* 2019, *14*, 1–18.

(11) Heisig, P.; Tschorny, R. Characterization of Fluoroquinolone-Resistant Mutants of Escherichia Coli Selected in Vitro. *Antimicrob. Agents Chemother.* 1994, *38*, 1284–1291.

(12) Collin, F.; Karkare, S.; Maxwell, A. Exploiting Bacterial DNA Gyrase as a Drug Target: Current State and Perspectives. *Appl. Microbiol. Biotechnol.* 2011, *92*, 479–497.

(13) Klostermeier, D. Towards Conformation-Sensitive Inhibition of Gyrase: Implications of Mechanistic Insight for the Identification and Improvement of Inhibitors. *Molecules* 2021, *19*.

(14) Oliphant, C. M.; Green, G. M. Quinolones: A Comprehensive Review. *Am. Fam. Physician* 2002, *65*, 455–464.

(15) Kolarič, A.; Anderluh, M.; Minovski, N. Two Decades of Successful SAR-Grounded Stories of the Novel Bacterial Topoisomerase Inhibitors (NBTIs). *J. Med. Chem.* 2020, *63*, 5664–5674.

(16) Flatman, R. H.; Eustaquio, A.; Li, S. M.; Heide, L.; Maxwell, A. Structure-Activity Relationships of Aminocoumarin-Type Gyrase and Topoisomerase IV Inhibitors Obtained by Combinatorial Biosynthesis. *Antimicrob. Agents Chemother.* 2006, *50*, 1136–1142.

(17) Edwards, M. J.; Flatman, R. H.; Mitchenall, L. A.; Stevenson, C. E. M.; Le, T. B. K.; Clarke, T. A.; McKay, A. R.; Fiedler, H.-P.; Buttner, M. J.; Lawson, D. M.; Maxwell, A. A Crystal Structure of the Bifunctional Antibiotic Simocyclinone D8, Bound to DNA Gyrase. *Science.* 2009, No. December, 1415–1419.

(18) Dalhoff, A. Global Fluoroquinolone Resistance Epidemiology and Implictions for Clinical Use. *Interdiscip. Perspect. Infect. Dis.* 2012, *2012*.

(19) Redgrave, L. S.; Sutton, S. B.; Webber, M. A.; Piddock, L. J. V. Fluoroquinolone Resistance: Mechanisms, Impact on Bacteria, and Role in Evolutionary Success. *Trends Microbiol.* 2014, *22*, 438–445.

(20) Saarukka, L.; Viljemaa, K.; Backman, J.; Blom, M. Fluoroquinolone-Related Adverse Events Resulting In Health Care Use And Costs: A Systematic Review. *Value Heal.* 2017, *20*, A669–A670.

(21) Kolarič, A.; Minovski, N. Novel Bacterial Topoisomerase Inhibitors: Challenges and Perspectives in Reducing HERG Toxicity. *Future Med. Chem.* 2018, *10*, 2241–2244.

(22) Baba, T.; Ara, T.; Hasegawa, M.; Takai, Y.; Okumura, Y.; Baba, M.; Datsenko, K. A.; Tomita, M.; Wanner, B. L.; Mori, H. Construction of Escherichia Coli K-12 In-frame, Single-gene Knockout Mutants: The Keio Collection. *Mol. Syst. Biol.* 2006, *2*.

(23) Seierstad, M.; Tichenor, M. S.; Desjarlais, R. L.; Na, J.; Bacani, G. M.; Chung, D. M.; Mercado-Marin, E. V; Steffens, H. C.; Mirzadegan, T. Novel Reagent Space: Identifying Unorderable but Readily Synthesizable Building Blocks. *ACS Med. Chem. Lett. 2021* 1853, *12*, 59.

(24) Green, M. R.; Sambrook, J. *Molecular Cloning: A Laboratory Manual*; 2012.

(25) Li, H.; Durbin, R. Fast and Accurate Short Read Alignment with Burrows-Wheeler Transform. *Bioinformatics* 2009, *25*, 1754–1760.

(26) Li, H.; Handsaker, B.; Wysoker, A.; Fennell, T.; Ruan, J.; Homer, N.; Marth, G.; Abecasis, G.; Durbin, R. The Sequence Alignment/Map Format and SAMtools. *Bioinformatics* 2009, *25*, 2078–2079.

(27) Wang, K.; Li, M.; Hakonarson, H. ANNOVAR: Functional Annotation of Genetic Variants from High-Throughput Sequencing Data. *Nucleic Acids Res.* 2010, *38*, 1–7.

(28) Jiang, Y.; Chen, B.; Duan, C.; Sun, B.; Yang, J.; Yang, S. Multigene Editing in the Escherichia Coli Genome via the CRISPR-Cas9 System. *Appl. Environ. Microbiol.* 2015, *81*, 2506–2514.
(29) Odds, F. C. Synergy, Antagonism, and What the Chequerboard Puts between Them. *J. Antimicrob. Chemother.* 2003, *52*, 1–1.
(30) Punjani, A.; Rubinstein, J. L.; Fleet, D. J.; Brubaker, M. A. CryoSPARC: Algorithms for Rapid Unsupervised Cryo-EM Structure Determination. *Nat. Methods* 2017, *14*, 290–296.
(31) Punjani, A.; Zhang, H.; Fleet, D. J. Non-Uniform Refinement: Adaptive Regularization Improves Single-Particle Cryo-EM Reconstruction. *Nat. Methods* 2020, *17*, 1214–1221.
(32) Zivanov, J.; Nakane, T.; Scheres, S. H. W. Estimation of High-Order Aberrations and Anisotropic Magnification from Cryo-EM Data Sets in RELION-3.1. *IUCrJ* 2020, *7*, 253–267.
(33) Pettersen, E. F.; Goddard, T. D.; Huang, C. C.; Meng, E. C.; Couch, G. S.; Croll, T. I.; Morris, J. H.; Ferrin, T. E. UCSF ChimeraX: Structure Visualization for Researchers, Educators, and Developers. *Protein Sci.* 2021, *30*, 70–82.
(34) Emsley, P.; Lohkamp, B.; Scott, W. G.; Cowtan, K. Features and Development of Coot. *Acta Crystallogr.* 2010, *D66*, 486–501.
(35) Liebschner, D.; Afonine, P. V.; Baker, M. L.; Bunkoczi, G.; Chen, V. B.; Croll, T. I.; Hintze, B.; Hung, L. W.; Jain, S.; McCoy, A. J.; Moriarty, N. W.; Oeffner, R. D.; Poon, B. K.; Prisant, M. G.; Read, R. J.; Richardson, J. S.; Richardson, D. C.; Sammito, M. D.; Sobolev, O. V.; Stockwell, D. H.; Terwilliger, T. C.; Urzhumtsev, A. G.; Videau, L. L.; Williams, C. J.; Adams, P. D. Macromolecular Structure Determination Using X-Rays, Neutrons and Electrons: Recent Developments in Phenix. *Acta Crystallogr.* 2019, *D75*, 861–877.
(36) Williams, C.; Headd, J.; Moriarty, N.; Prisant, M.; Videau, L.; Deis, L.; Verma, V.; Keedy, D.; Hintze, B.; Chen, V.; Jain, S.; Lewis, S.; Arendall, W.; Snoeyink, J.; Adams, P.; Lovell, S.; Richardson, J.; Richardson, D. MolProbity: More and Better Reference Data for Improved All-atom Structure Validation. *Protein Sci.* 2018, *27*, 293–315.
(37) Schindelin, J.; Arganda-Carreras, I.; Frise, E.; Kaynig, V.; Longair, M.; Pietzsch, T.; Preibisch, S.; Rueden, C.; Saalfeld, S.; Schmid, B.; Tinevez, J. Y.; White, D. J.; Hartenstein, V.; Eliceiri, K.; Tomancak, P.; Cardona, A. Fiji: An Open-Source Platform for Biological-Image Analysis. *Nat. Methods* 2012, *9*, 676–682.
(38) Berg, S.; Kutra, D.; Kroeger, T.; Straehle, C. N.; Kausler, B. X.; Haubold, C.; Schiegg, M.; Ales, J.; Beier, T.; Rudy, M.; Eren, K.; Cervantes, J. I.; Xu, B.; Beuttenmueller, F.; Wolny, A.; Zhang, C.; Koethe, U.; Hamprecht, F. A.; Kreshuk, A. Ilastik: Interactive Machine Learning for (Bio)Image Analysis. *Nat. Methods* 2019, *16*, 1226–1232.
(39) Ducret, A.; Quardokus, E. M.; Brun, Y. V. MicrobeJ, a Tool for High Throughput Bacterial Cell Detection and Quantitative Analysis. *Nat. Microbiol.* 2016, *1*, 1–7.